4.8 GHz to 5.3 GHz and return losses of both antennas within this frequency range are around -10 dB. These results further verify our design and allow the practical implementation of the SWTLA.

IV. Conclusion

We have successfully extended the surface wave control technology into the antenna engineering and proposed a new class of DSRs as SWTLAs for enhanced end-fire radiation. A potential realization of such SWTLAs through the perforated design has been demonstrated with an emphasis especially on the tradeoff in antenna performance and the required unit cell numbers in the practical implementation. Numerical results from full wave simulations have validated the functionality of our proposed SWTLAs that are able to efficiently convert the spherical surface wave into the plane surface wave and thus greatly improve the antenna directivity. The present approach, based on a contemporary theory of transformation optics, provides a new route to design SWAs, thus leading to potential innovations in the design of other functional devices that are fundamentally dependent on the creeping wave propagation.

References

[1] F. E. Butterfield, "Dielectric sheet radiators," *IRE Trans. Antennas Propag.*, vol. 2, no. 4, pp. 152–158, 1954.

[2] L. B. Felson, "Radiation from a tapered surface wave antenna," *IRE Trans. Antennas Propag.*, vol. 8, no. 6, pp. 577–586, 1960.

[3] R. E. Collin, *Field Theory of Guided Waves*. New York, NY, USA: Wiley-IEEE Press, 1990.

[4] D. M. Pozar, *Microwave Engineering*. Hoboken, NJ, USA: Wiley, 2005.

[5] H. Barlow and A. Cullen, "Surface waves," in *Proc. IEE*, 1953, vol. 100, pp. 329–347.

[6] F. J. Zucker, , R. C. Johnson, Ed., "Surface-wave antennas," in *Antenna Engineering Handbook*, 3rd ed. New York, NY, USA: McGraw-Hill, 1993, ch. 12.

[7] J. D. Kraus and R. J. Marhefka, *Antennas for All Applications*, 3rd ed. New York, NY, USA: McGraw, 2001.

[8] C. H. Walter, "Surface wave Luneberg lens antenna," *IRE Trans. Antennas Propag.*, vol. 8, no. 5, pp. 508–515, 1960.

[9] R. E. Plummer, "Surface wave beacon antenna," *IRE Trans. Antennas Propag.*, vol. 6, no. 1, pp. 105–114, 1958.

[10] R. W. Hougardy and R. C. Hansen, "Scanning surface wave antennas C oblique surface waves over a corrugated conductor," *IRE Trans. Antennas Propag.*, vol. 6, no. 4, pp. 370–376, 1958.

[11] S. Maci, G. Minatti, M. Casaletti, and M. Bosiljevac, "Metasurfing: Addressing waves on impenetrable metasurfaces," *IEEE Antennas Wireless Propag. Lett.*, vol. 10, pp. 1499–1502, 2011.

[12] M. Bosiljevac, M. Casaletti, F. Caminita, Z. Sipus, and S. Maci, "Non-uniform metasurface Luneburg lens antenna design," *IEEE Trans. Antennas Propag.*, vol. 60, no. 9, pp. 4065–4073, 2012.

[13] F. Yang, Y. Rahmat-Samii, and A. Kishk, "Low-profile patch-fed surface wave antenna with a monopole-like radiation pattern," *IET Microw. Antennas Propag.*, vol. 1, no. 1, pp. 261–266, 2007.

[14] F. Yang, A. Kish, and Y. Rahmat-Samii, "A novel surface wave antenna design using a thin periodically loaded ground plane," *Microw. Opt. Technol. Lett.*, vol. 47, no. 3, pp. 240–245, 2005.

[15] R. Yang and Y. Hao, "An accurate control of the surface wave using transformation optics," *Opt. Express*, vol. 20, no. 9, pp. 9341–9350, 2012.

[16] J. Li and J. B. Pendry, "Hiding under the carpet: A new strategy for cloaking," *Phys. Rev. Lett.*, vol. 101, no. 20, p. 203901, 2008.

[17] D. Schurig, J. B. Pendry, and D. R. Smith, "Calculation of material properties and ray tracing in transformation media," *Opt. Express*, vol. 14, no. 21, pp. 9794–9804, 2006.

[18] E. Kallos, C. Argyropoulos, and Y. Hao, "Ground-plane quasicloaking for free space," *Phys. Rev. A*, vol. 79, no. 6, p. 063825, 2009.

[19] R. Yang, W. X. Tang, Y. Hao, and I. Youngs, "A coordinate transformation based broadband flat lens via microstrip array," *IEEE Antennas Wireless Propag. Lett.*, vol. 10, pp. 99–102, 2011.

[20] R. Yang, W. X. Tang, and Y. Hao, "Wideband beam-steerable flat reflectors via transformation optics," *IEEE Antennas Wireless Propag. Lett.*, vol. 10, pp. 1290–1294, 2011.

[21] R. Yang, Z. Y. Lei, L. Chen, J. W. Zhang, Z. X. Wang, and Y. J. Xie, "Broadband converging plano-concave lens," *Opt. Lett.*, vol. 38, no. 13, pp. 2311–2313, 2013.

[22] R. Yang, W. X. Tang, and Y. Hao, "A broadband zone plate lens from transformation optics," *Opt. Express*, vol. 19, no. 13, pp. 12348–12355, 2011.

[23] H. F. Ma and T. J. Cui, "Three-dimensional broadband and broad-angle transformation-optics lens," *Nat. Commun.*, vol. 8, p. 124, 2010.

[24] A. Petosa and A. Ittipiboon, "Design and performance of a perforated dielectric Fresnel lens," *IEE Proc. Microw. Antennas Propag.*, vol. 150, no. 5, pp. 309–314, 2003.

[25] D. R. Smith, D. C. Vier, Th. Koschny, and C. M. Soukoulis, "Electromagnetic parameter retrieval from inhomogeneous metamaterials," *Phys. Rev. E, Stat. Nonlin. Soft Matter Phys.*, vol. 71, no. 3, p. 036617, 2005.

Low Profile Vertically Polarized Omnidirectional Wideband Antenna With Capacitively Coupled Parasitic Elements

Jungsuek Oh and Kamal Sarabandi

***Abstract*—This communication presents a low profile and electrically small wideband antenna with omnidirectional radiation pattern and vertical polarization. A novel design approach manipulating the topology of a low profile folded monopole antenna with capacitively coupled parasitic elements in the same plane is presented to achieve omnidirectional radiation pattern. The 10-dB return loss fractional bandwidth of 43% is achieved with the dimension of $0.2\lambda_{LF} \times 0.2\lambda_{LF} \times 0.06\lambda_{LF}$ where λ_{LF} is the wavelength at the lowest frequency of the operation. Unlike the convention wideband $\lambda/4$ monopole antennas utilizing inductively coupled parasitic elements, the $\lambda/2$ folded monopole antenna allows for positioning the capacitively coupled parasitic elements in the middle of the antenna where maximum electric stored energy is formed. This, together with reducing the lateral dimension of the folded monopole antenna, enables the cancellation of radiated fields from electric currents in the horizontal plane of the proposed antenna, which is essential to achieve vertically polarized omnidirectional radiation. The compact parasitic elements introduce additional resonances that significantly increase the antenna bandwidth. Effects of design parameters on two resonant frequencies and impedance matching to a 50 Ω feed are investigated using the equivalent circuit model of the parasitic element and full-wave electromagnetic (EM) simulations. Based on this analysis, a design procedure to optimize the antenna topology is established.**

***Index Terms*—Broadband antennas, electrically small antennas, omnidirectional antennas.**

I. Introduction

Broadband antennas with vertically polarized omnidirectional radiation pattern in the azimuthal plane have attracted significant attention for their applications in wireless communications such as unattended ground sensor networks and wireless local area network

Manuscript received October 01, 2012; revised October 07, 2013; accepted November 12, 2013. Date of publication November 20, 2013; date of current version January 30, 2014. This work was supported in part by the U.S. Army Research Laboratory under contract W911NF and prepared through collaborative participation in the Microelectronics Center of Micro Autonomous Systems and Technology (MAST) Collaborative Technology Alliance (CTA) and NSF under contract ECCS1101868.

The authors are with the Radiation Laboratory, Department of Electrical Engineering and Computer Science, The University of Michigan at Ann Arbor, Ann Arbor, MI 48109-2122 USA (e-mail: jungsuek@umich.edu; saraband@eecs.umich.edu).

Color versions of one or more of the figures in this communication are available online at http://ieeexplore.ieee.org.

Digital Object Identifier 10.1109/TAP.2013.2291891

(WLAN) systems [1]–[5]. Vertical polarization is important for near-ground applications in so far as the path-loss is concerned and omnidirectional radiation characteristic is needed for wide coverage in all directions. It is reported that near-ground propagation path loss between two near-ground antennas for vertically oriented antennas is by many orders of magnitude lower than any other antenna orientation configurations [6]–[8]. Quarter-wave ($\lambda/4$) monopole antenna is a typically used for near-ground communication applications. However, the size of the ground plane must be large, antenna height may be prohibitively large ($\lambda/4$) and its bandwidth is relatively low ($<$10%). The literature concerning antenna miniaturization is vast but far less for low profile, electrically small, wideband and vertically polarized antennas [21]. Many different types of low-profile inverted-F antenna have been the most commonly used [9], [10]. However, in most of such antenna topologies, only a short vertical segment of the resonant structure contributes to the vertically polarized radiation, while much larger portion of the antenna structure generates higher radiation with undesired polarizations. This causes poor polarization purity and a serious deformation in the desired omnidirectional radiation pattern [11], [22]. Recently, a new type of low-profile antenna with omnidirectional radiation pattern and vertical polarization was reported [12]. The concept is based on a superposition of multiple quarter-wave segments that are meandered and spiraled around to suppress the radiation from horizontal currents above the ground plane. As a result, the antenna features a pure vertically polarized radiation in the horizontal plane.

Various types of multiband and wideband inverted-F antennas with parasitic elements have also been reported [13]–[16]. In these papers inverted-L parasitic elements are inductively coupled to the inverted-F antennas to enhance the bandwidth. The inductively coupled parasitic element method for improving the bandwidth is widely used because of its simplicity in design and ease of integration with inverted-F antennas. In order to achieve the required level of inductive coupling, the parasitic elements are positioned close to the feeding segment of the inverted-F antennas, which perturbs the uniformity of radiation pattern. In addition, similar to ordinary inverted-F antennas, these antennas are in capable of generating pure vertical polarization in the horizontal plane of the antenna.

This communication presents a novel antenna topology that makes use of capacitively coupled parasitic elements to achieve broad bandwidth without perturbing omnidirectional radiation pattern or the polarization of the antenna. The proposed antenna is a meandered $\lambda/2$ folded (bent over a ground plane) monopole antenna coupled capacitively to the parasitic elements. In Section II-A, the behavior of the input impedance of the capacitively coupled parasitic element is studied based on its equivalent circuit model. In Section II-B, the resonant modes of the antenna with a parasitic element as a function of the parasitic element parameters are determined based on which a design procedure is developed. In Section III-A, geometrical optimization of the antenna structure is presented to achieve omnidirectional radiation pattern and impedance matching to a 50 Ω feed. In Section III-B, a meandered $\lambda/2$ folded monopole antenna with a single parasitic element is designed. In Section III-C, the bandwidth of antenna is enhanced by introducing an additional capacitive coupled parasitic element.

II. Circuit Analysis of Folded Monopole Antenna With Capacitively Coupled Parasitic Element

A. Equivalent Circuit Model of Capacitively Coupled Parasitic Element

A $\lambda/2$ folded monopole antenna is used as a starting point for the proposed wideband, omnidirectional, vertically polarized antenna with small dimensions. Here the $\lambda/2$ folded monopole antenna refers to a short circuited microstrip transmission line fed from one end of a vertical pin. The bandwidth of the folded monopole antenna based on $\lambda/2$ transmission line (TRL) is wider than that of the conventional $\lambda/4$ inverted F antennas, just as the bandwidth of $\lambda/2$ folded dipole antenna is 2$\sim$3 times wider than ordinary $\lambda/2$ dipole antenna [16], [17]. In addition, modifying the antenna topology to be fitted in a small area allows for omnidirectional radiation pattern, as will be discussed in Section III-A. This section presents the operation of the capacitively coupled parasitic element to excite an additional resonant frequency (f_{low}) lower than the original operating frequency (f_{high} where $f_{high} > f_{low}$) of the folded monopole antenna. Positioning the two resonant frequencies close to each other results in increasing the bandwidth of the antenna. It is shown that this can be done by adding a reactive parasitic element. Let us consider the required antenna configuration to excite the resonance at f_{low}. The original operating frequency (f_{high}) can be moved down to f_{low} by adding a series inductor or a shunt capacitor to the transmission line as shown in Fig. 1(a) and (b) due to an additional phase shift through the reactive elements. Our goal is to design a proper reactive parasitic element supporting two resonant frequencies (f_{low} and f_{high}) simultaneously as a way to enhance the bandwidth. It is proposed to simultaneously excite both resonant modes by positioning an inverted-L parasitic element with proper length and distance near the middle of the $\lambda/2$ folded monopole antenna where the electric filed is maximum. Because of the high electric field in the middle of the antenna, the antenna can establish a strong capacitive coupling with a parasitic element at that location. Counter-intuitively, the short-circuited end is placed near the folded antenna in order to excite the desired mode. In this way, the short-circuited end that acts as an inductor appears as a shunt element to the open-ended stub and are both connected to the series parasitic capacitance. It must be noted that metallic traces in the antenna are represented by pure reactive elements in the circuit model to investigate the resonant properties as a function of design parameters.

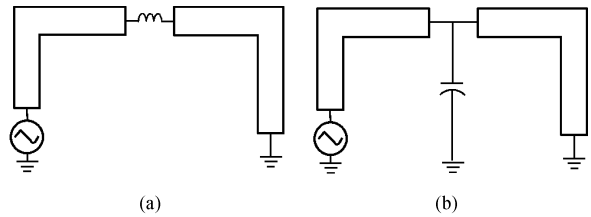

Fig. 1. Folded monopole antennas with (a) a series inductor and (b) a shunt capacitor to excite a lower resonant frequency (f_{low}).

Fig. 2(a) shows the $\lambda/2$ folded monopole antenna capacitively coupled to the inverted-L parasitic element where $h = 60$ mm, $w_{TRL} = 30$ mm, $w_{par} = 60$ mm, $L_{par} = 150$ mm and the gap between the $\lambda/2$ folded monopole antenna and the parasitic element $= 15$ mm. Fig. 2(b) shows an equivalent circuit model of the parasitic element. Input impedance (Z_{in}) of the equivalent circuit model can be found from

$$Z_{in} = \frac{L_1L_2C_1C_2\omega^4 - (L_1C_1 + L_1C_2 + L_2C_2)\omega^2 + 1}{jwC_1\left(1 - (L_1C_2 + L_2C_2)\omega^2\right)}. \quad (1)$$

At $\omega = 1/\sqrt{L_1C_2 + L_2C_2}$ where $\omega = 2\pi f$, Z_{in} is infinite and thus no electric currents are induced on the parasitic element. As a result, the antenna works as if the parasitic element doesn't exist. On the other hand, at frequencies where $\omega < \sqrt{(Y - \sqrt{Y^2 - 4/(L_1L_2C_1C_2)})/2}$, $\mathrm{Im}(Z_{in})$ becomes negative (capacitive), noting that $Y = 1/(L_1C_1) + 1/(L_2C_1) + 1/(L_2C_2)$. In this case, the antenna structure works the

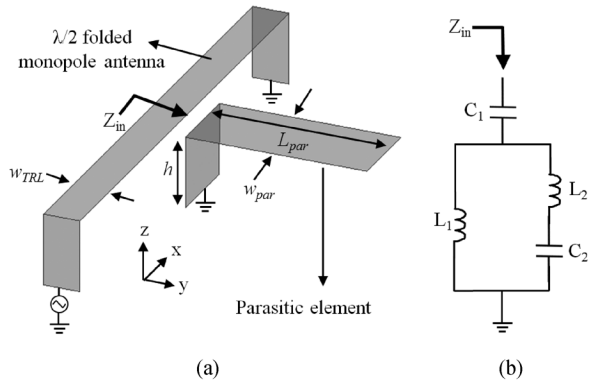

Fig. 2. (a) Perspective view of a $\lambda/2$ folded monopole antenna with a capacitively coupled parasitic element and (b) the equivalent circuit model of the parasitic element.

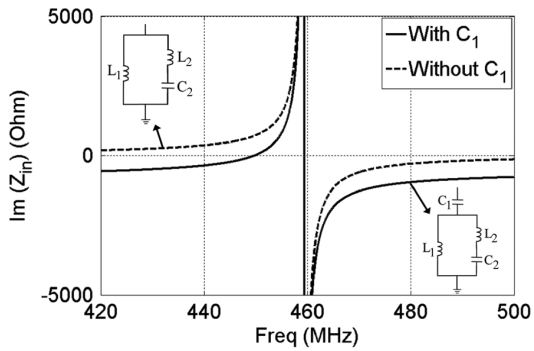

Fig. 3. Imaginary part of Z_{in} in the equivalent circuit model of the capacitively coupled parasitic element shown in Fig. 2(b), compared to the same circuit model without C_1.

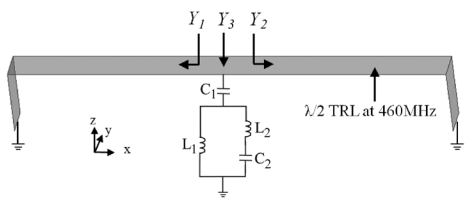

Fig. 4. Input admittances toward two shorting strips and the parasitic element in the middle of a shorted $\lambda/2$ TRL.

same way as the topology shown in Fig. 1(b). Therefore, the use of the capacitively coupled inverted-L parasitic element enables the operations corresponding to two resonant frequencies (f_{low} and f_{high}) simultaneously. In order to further investigate the operation of the capacitively coupled parasitic element, the imaginary part of Z_{in} of the equivalent circuit model of the parasitic element is compared with that of the circuit without the coupled capacitance (C_1), as shown in Fig. 3. The values of the lumped elements are chosen as $C_1 = 0.5$ pF, $L_1 = 20$ nH, $C_2 = 3$ pF and $L_2 = 20$ nH, approximately corresponding to physical dimensions of the parasitic element for frequency of operation at $f_{high} = 460$ MHz [18]–[20]. It is found that below 460 MHz the imaginary part of Z_{in}, in the presence of C_1, becomes negative (capacitive). This is desirable since it allows excitation of an additional resonance at a frequency lower than 460 MHz, as discussed earlier. The physical length of the folded monopole antenna is designed to be $\lambda/2$ at 460 MHz (f_{high}) that must match the pole of (1) given by $f_{pol} = 1/(2\pi\sqrt{L_1C_2 + L_2C_2})$.

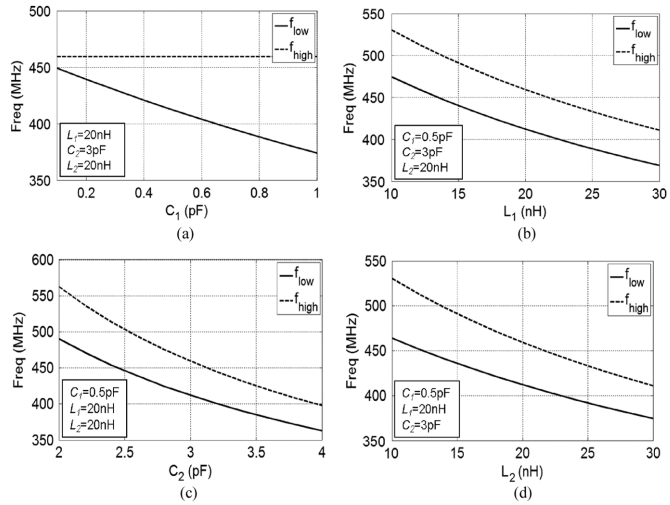

Fig. 5. f_{low} and f_{high} versus (a) C_1, (b) L_1, (c) C_2 and (d) L_2 in the equivalent circuit model of the parasitic element in Fig. 4. A text box in each plot shows the fixed values of other parameters.

B. Parametric Study

In order to develop a design procedure for the proposed wideband antenna, it is essential to investigate the characteristics of the two resonant frequencies as a function of design parameters of the parasitic element. The design parameters are the gap between the $\lambda/2$ folded monopole antenna and the parasitic element (corresponding to C_1 in Fig. 2(b)), the width and height of the shorting strip (L_1) and the geometry of the top plate (C_2 and L_2). Another important parameter is the characteristic mode of the antenna structure. To determine the resonant frequencies the transverse resonance technique can be used. This technique requires that the sum of the input admittances (impedances) seen looking into either sides at any point along the transmission line be zero at resonant frequencies of the transmission line where voltage and current standing waves are formed. That is

$$Y_{in}^{r}(x) + Y_{in}^{l}(x) = 0, \qquad \text{for all } x \tag{2}$$

where $Y_{in}^{r}(x)$ and $Y_{in}^{l}(x)$ are the input admittances seen looking to the right and left, respectively, at the point x on the resonant TRL. Referring to Fig. 5, this condition renders

$$\frac{1}{jZ_0 \tan\beta_0 l} + \frac{1}{jZ_0 \tan\beta_0 l} + \frac{j\omega C_1\left(1 - (L_1C_2 + L_2C_2)w^2\right)}{L_1L_2C_1C_2\omega^4 - (L_1C_1 + L_1C_2 + L_2C_2)\omega^2 + 1} = 0 \tag{3}$$

where Z_0 is the characteristic impedance of the TRL (chosen as 200 Ω), β_0 is the propagation constant in free space and l is $\lambda_0/4$ at 460 MHz (λ_0 is free-space wavelength).

The solutions of (3) give the two resonant frequencies (f_{low} and f_{high}) as a function of C_1, L_1, C_2 and L_2, as shown Fig. 5. Except for the lumped element under parametric study, all other values are fixed as the same values used in Section II-A. Fig. 5(a) shows that as C_1 increases, f_{low} decreases while f_{high} doesn't change as expected. This means that the change in the gap distance between the $\lambda/2$ folded monopole antenna and the parasitic element only results in the shift of f_{low}. On the other hand, Fig. 5(b), (c) and (d) suggest that the increase in L_1, C_2 or L_2 leads to the decrease in f_{high} as well as f_{low}. This is due to the fact that the pole of (1) is a function of L_1, C_2 and L_2 and thus once their value is changed, the pole of (1) is not equal to the

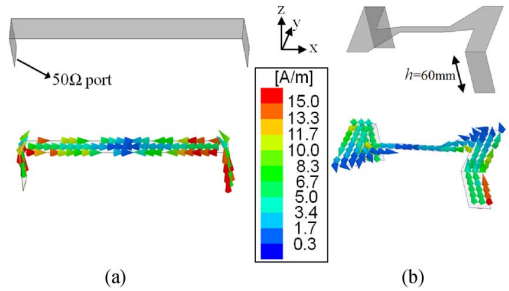

Fig. 6. Geometries and electric current distributions of (a) straight and (b) meandered $\lambda/2$ folded monopole antenna.

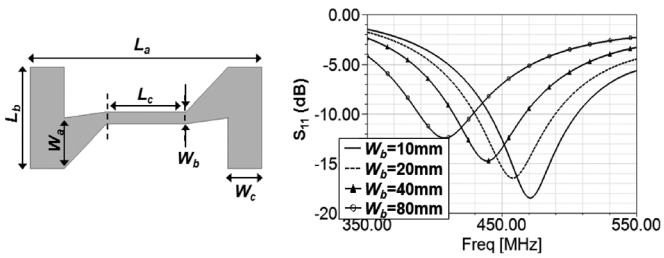

Fig. 7. (a) Design parameters of meandered $\lambda/2$ folded monopole antenna and (b) simulated S_{11} of the modified folded monopole geometry as a function of width parameter (W_b).

frequency at which the electrical length of the folded monopole antenna is seen as $\lambda/2$ any longer. As a result, the $f_{\rm high}$ moves down to satisfy the resonant condition of (3).

It is expected that both f_{low} and f_{high} can be decreased by increasing the area of the top plate along y-axis or decreasing the width of the shorting strip of the parasitic element. Based on this parametric study, a design procedure to optimize the geometry of the parasitic element can be established. Firstly, for a given lateral dimensions, the area of the top plate of the parasitic element needs to be maximized to lower both f_{low} and f_{high}, leading to antenna miniaturization. Secondly, L_1 is tuned to make the pole of (1) to be positioned around the frequency at which the electrical length of the folded monopole antenna is seen as $\lambda/2$. Next, since the change of C_1 only affects f_{low}, the desired separation between f_{low} and f_{high} can be set to maximize the bandwidth for a desired minimum return loss. The frequency separation can be adjusted by controlling the gap distance between the antenna and the parasitic element.

III. Antenna Design

A. Design of Meandered Folded Monopole Antenna

This section presents the geometry optimization of the $\lambda/2$ folded monopole antenna to achieve omnidirectional radiation pattern and impedance matching to a 50 Ω feed. Fig. 6 shows the geometries and electric current distributions over a straight $\lambda/2$ folded monopole antennas matched to a 50 Ω port. Since the separation between the two vertical pins of the antenna is $\lambda/2$ and the electric currents on the vertical pins are in-phase, there is an undesired cancellation of vertically polarized radiation along the x-axis. In order to achieve omnidirectional radiation pattern in the horizontal plane (xy plane), the lateral dimension of the antenna must be reduced to avoid the radiation cancellation. Meanwhile, the polarization purity of the straight $\lambda/2$ folded monopole antenna must be maintained. As shown in Fig. 6(a), horizontal electric currents on the left side of the top plate are in the opposite direction of those on the right side. This suppresses

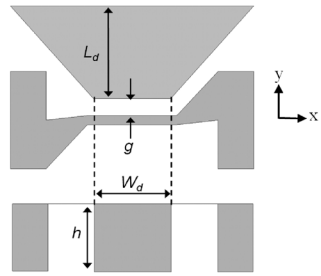

Fig. 8. Top/side view and design parameters of the meandered $\lambda/2$ folded monopole antenna with the capacitively coupled parasitic element.

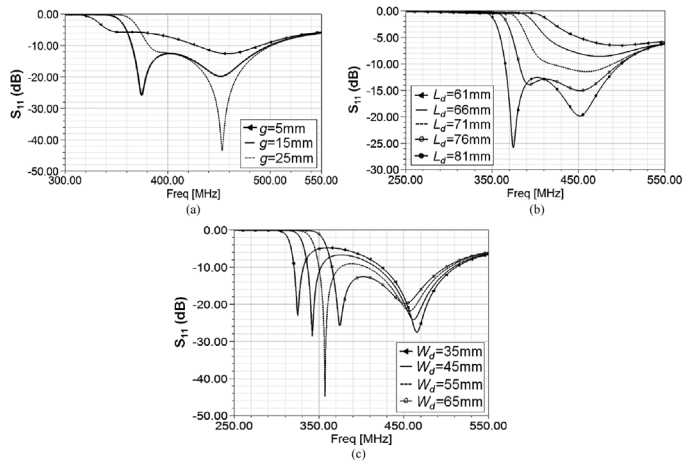

Fig. 9. Simulated S_{11} of the proposed antenna as a function of (a) g, (b) L_d and (c) W_d.

the radiated fields with undesired (horizontal) polarization from the metallic trace on the top plate. This desired property can be maintained by making the metallic trace meander in the way shown in Fig. 6(b). Fig. 7(a) shows the design parameters of the antenna geometry. Since a short segment (L_c) can work as an impedance transformer, impedance matching to a 50 Ω feed can be obtained by tuning L_c and W_b. Fig. 7(b) shows the simulated S_{11} as a function of W_b where the values of other parameters are fixed as $L_a = 200$ mm, $L_b = 85$ mm, $L_c = 70$ mm, $W_a = 42.5$ mm and $W_c = 30$ mm. For the full-wave electromagnetic (EM) simulations, Ansoft HFSS 13.0 is used.

B. Design of Meandered Folded Monopole Antenna With One Parasitic Element

The capacitively coupled parasitic element combined with the meandered $\lambda/2$ folded monopole antenna is optimized, based on the design procedure proposed in Section II-B. Fig. 8 shows three design parameters determining the geometry of the parasitic element. In order to maximize C_2 and L_2 in Fig. 2(b) for a given area, a trapezoid-shaped top plate is chosen. Once the value of L_d is decided, the value of W_d is appropriately chosen to make the pole of (1) to be positioned around the frequency at which the electrical length of the folded monopole antenna is $\lambda/2$. The proper separation between f_{low} and f_{high} can be designed by tuning the gap distance g because C_1 only affects f_{low}. Changing W_d and g slightly, excellent impedance matching to a 50 Ω feed at both f_{low} and f_{high} is obtained. Fig. 9 shows simulated S_{11} as a function of g, L_d and W_d. The initial values used for this study are $g = 15$ mm, $L_d = 81$ mm, $W_d = 65$ mm and $h = 60$ mm. As expected, while the change in g only affects f_{low}, the change in L_d changes both f_{low} and f_{high}, showing the behavior predicted by circuit simulations. On the other hand, decreasing W_d only lowers f_{low},

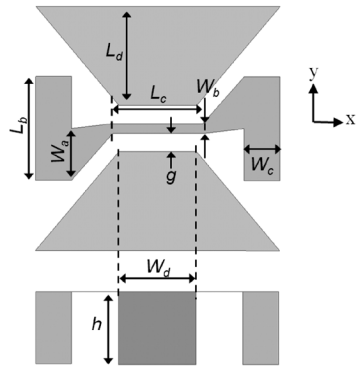

Fig. 10. Top/side view and design parameters of the proposed omnidirectional antenna topology with two back-to-back parasitic elements.

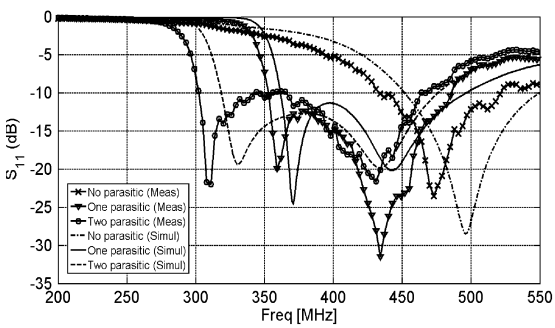

Fig. 11. Simulated and measured S_{11} of the proposed antenna corresponding to three cases: *i*. Antenna without any parasitic element ('no parasitic'), *ii*. Antenna with one parasitic element ('one parasitic') and *iii*. Antenna with two parasitic elements (denoted by 'two parasitic').

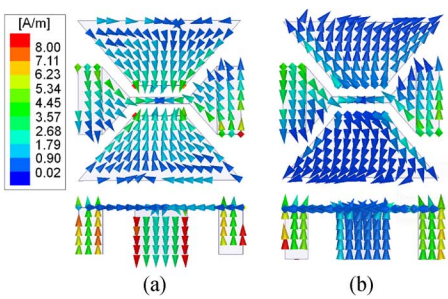

Fig. 12. Current distributions (top/side view) at (a) 330 MHz and (b) 430 MHz.

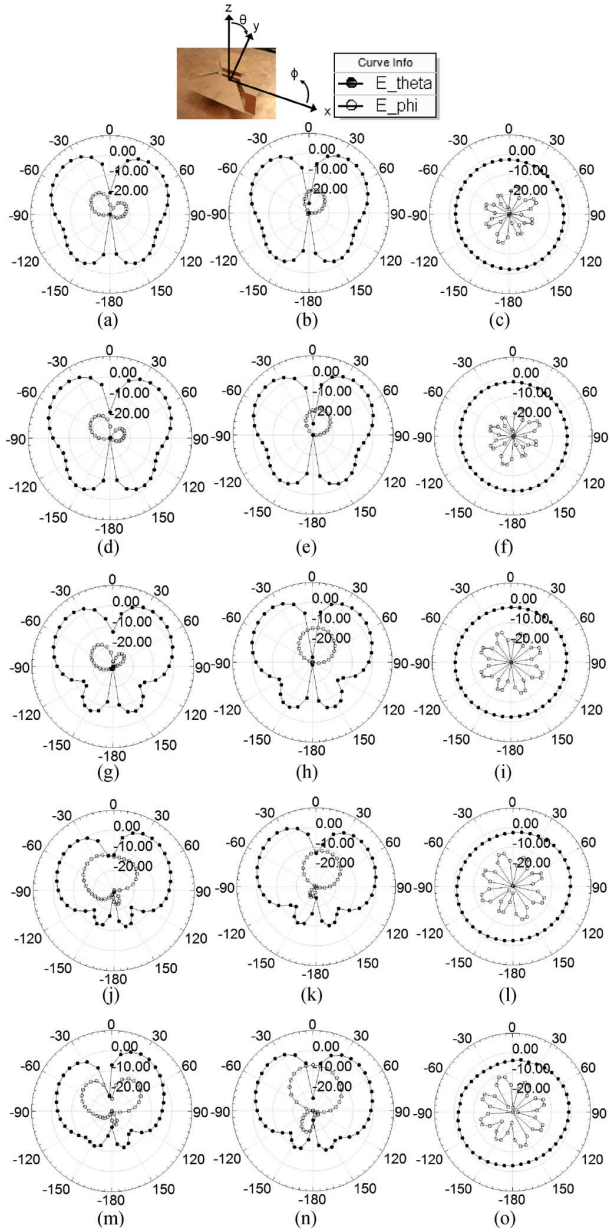

Fig. 13. Measured radiation patterns in xz (E)-plane, yz (E)-plane and xy (H)-plane at 320 (a–c), 330 (d–f), 380 (g–i), 430 (j–l) and 475 (m–o) MHz.

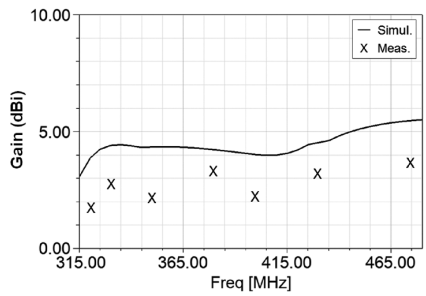

Fig. 14. Simulated and measured gain of the proposed antenna.

contrary to the circuit-model prediction where the increase in L_1 resulted in lowering both f_{low} and f_{high}. This difference is due to the fact that the change in W_d also causes a change in C_1 and the transition geometry between the shorting strip and the top plate.

C. Bandwidth Enhancement Using Two Back-to-Back Parasitic Elements

Introducing an additional parasitic element to the antenna topology with one parasitic element, as shown in Fig. 10, makes the antenna topology symmetric with respect to the E plane (xz plane). This has a potential to enhance radiation pattern of the antenna. Noting that the electric currents on the horizontal plane of the second parasitic element are in the opposite direction of those on the first parasitic element ensures cancellation of horizontally polarized radiated fields from the first and second parasitic elements. This enhances the polarization purity of the vertically polarized antenna. The addition of the second parasitic element with identical dimensions does not change the circuit model and the principle of operation, but it allows storage of electric and magnetic energy over a larger volume, which should result in wider bandwidth. In addition, tuning the dimensions of the second parasitic

element provides the opportunity to excite another resonance. Considering the second parasitic element with dimensions identical to those of the first element, as discussed in the previous section, the performance of the modified antenna is studied.

Fig. 10 shows the geometry and design parameters of the modified antenna topology. In order to compensate the slight change in impedance matching due to the addition of the second parasitic element, W_a is adjusted. The values of design parameters are given by $L_a = 200$ mm, $L_b = 85$ mm, $L_c = 75$ mm, $L_d = 81$ mm, $W_a = 85$ mm, $W_b = 8$ mm, $W_c = 30$ mm, $W_d = 65$ mm, $g = 15$ mm and $h = 60$ mm. The size of the ground plane used for both the simulations and measurements is $0.7\lambda_{\rm LF} \times 0.7\lambda_{\rm LF} (= 70\ {\rm cm})$ where $\lambda_{\rm LF}$ is the wavelength at the lowest frequency of the operation. It must be noted that similar to any monopole-type antenna, as the size of the ground plane decreases the impedance matching becomes poor and the gain drops. Fig. 11 shows the simulated and measured S_{11} corresponding to three cases: *i*. Antenna without any parasitic element (denoted by 'no parasitic'), *ii*. Antenna with one parasitic element ('one parasitic') and *iii*. Antenna with two parasitic elements ('two parasitic'). Comparing the case of 'one parasitic' to the case of 'two parasitic', it is shown that the addition of the second parasitic element lowers both f_{low} and f_{high}, and enhance fractional bandwidth. Misalignment between the antenna and ground plane and limited tolerance of the fabrication process cause a slight disagreement between the simulated and measured results. Fig. 12 shows electric current distributions at 330 MHz and 430 MHz of the proposed antenna shown in Fig. 10 (Case *iii* in Fig. 11). As intended, all the electric currents in the horizontal plane of the antenna have a counterpart that is in the opposite direction, leading to the cancellation of the radiated fields from the top plate.

Figs. 13 and 14 show the measured radiation patterns and gain of the proposed antenna (Case *iii*) at various frequencies. Desired omnidirectional radiation patterns having a null in the broadside direction are observed. In the proposed antenna topology, although the lateral dimensions are much larger than the vertical profile, the overall ratios of $\rm co (= E_\theta)$ to $\rm cross (= E_\phi)$ polarization are higher than 10 dB in the antenna bandwidth.

IV. Conclusion

A novel, electrically small, low profile, vertically polarized, and omnidirectional wideband antenna is presented. It is shown that through the application of novel capacitively coupled parasitic elements, a wideband folded monopole antenna over a finite ground plane with fractional bandwidth of 43% with the dimensions of $0.2\lambda_{\rm LF} \times 0.2\lambda_{\rm LF} \times 0.06\lambda_{\rm LF}$ where $\lambda_{\rm LF}$ is the wavelength at the lowest frequency of the operation, can be designed. This antenna shows a high ratio of co- to cross-polarization, and omnidirectional radiation pattern. Through a circuit model and sensitivity analysis of the design parameters of the parasitic elements, a design procedure is developed and used for the geometry optimization. Simulated and measured results well validate the design procedure and expected performance of the proposed antenna.

References

[1] F. R. Hsiao and K. L. Wong, "Omnidirectional planar folded dipole antenna," *IEEE Trans. Antennas Propag.*, vol. 52, no. 7, pp. 1898–1902, Jul. 2004.

[2] S. Palud, F. Colombel, M. Himdi, and C. Le Meins, "Wideband omnidirectional and compact antenna for VHF/UHF band," *IEEE Antennas Wireless Propag. Lett.*, vol. 10, pp. 3–6, 2011.

[3] P. C. Bybi, G. Augustin, B. Jitha, C. K. Anandan, K. Vasudevan, and P. Mohanan, "A quasi-omnidirectional antenna for modern wireless communication gadgets," *IEEE Antennas Wireless Propag Lett*, vol. 7, pp. 505–508, 2008.

[4] K. L. Wong, S. W. Su, and C. L. Tang, "Broadband omnidirectional metal-plate monopole antenna," *IEEE Trans. Antennas Propag.*, vol. 53, no. 1, pp. 581–583, Jan. 2005.

[5] X. Chen, K. Huang, and X.-B. Xu, "A novel planar slot array antenna with omni directional pattern," *IEEE Trans. Antennas Propag.*, vol. 59, no. 12, pp. 4853–4857, Dec. 2011.

[6] D. Liao and K. Sarabandi, "Terminal-to-terminal hybrid full-wave simulation of low-profile, electrically-small, near-ground antennas," *IEEE Trans. Antennas Propag.*, vol. 56, no. 3, pp. 806–814, Mar. 2008.

[7] D. Liao and K. Sarabandi, "Optimization of low-profile antennas for applications in unattended ground sensor networks," *IEEE Trans. Antennas Propag.*, vol. 53, no. 11, pp. 3747–3756, Nov. 2005.

[8] K. Sarabandi and M. Casciato, "Efficient calculation of the fields of a dipole radiating above an impedance surface," *IEEE Trans. Antennas Propag.*, vol. 50, no. 9, pp. 1222–1235, Sep. 2002.

[9] T. Taga and K. Tsunoda, "Analysis of a planar inverted-F antenna by spatial network method," *IEICE*, vol. J74-B-2, no. 10, pp. 538–545, Oct. 1991.

[10] S. Sekine, T. Ito, N. Odachi, Y. Murakami, and H. Shoki, "Design method for a broadband inverted-F antenna by parallel resonance mode," *IEICE*, vol. J86-B, no. 9, pp. 1806–1815, Sep. 2003.

[11] J. Oh and K. Sarabandi, "Low profile, miniaturized, inductively coupled capacitively loaded monopole antenna," *IEEE Trans. Antennas Propag.*, vol. 60, no. 3, pp. 1206–1213, Mar. 2012.

[12] W. B. Hong and K. Sarabandi, "Low-profile, multi-element, miniaturized monopole antenna," *IEEE Trans. Antennas Propag.*, vol. 57, no. 1, pp. 72–80, Jan. 2009.

[13] H. Nakano, R. Suzuki, and J. Yamauchi, "Low-profile inverted-f antenna with parasitic elements on an infinite ground plane," *IEE Proc. Microw. Antennas Propag.*, vol. 145, no. 4, pp. 321–325, Aug. 1998.

[14] K. Oh and K. Hirasawa, "A dual-band inverted-L-folded-antenna with a parasitic wire," in *Proc. IEEE Antennas Propag. Int. Symp.*, Monterey, CA, USA, Jun. 2004, pp. 3131–3134.

[15] Z. Jianwu, Z. Yangyang, and G. Feng, "A novel folded inverted-F antenna with parasitic stub for TD-SCDMA systems," in *Proc. IEEE Int. Workshop on Antenna Technology*, 2009, pp. 1–4.

[16] K. B. Kim, H. K. Ryu, and J. M. Woo, "Compact wideband folded monopole antenna coupled with parasitic inverted-L element for laptop computer applications," *IET Electron. Lett.*, vol. 47, no. 5, pp. 301–303, Mar. 2011.

[17] M. Olmos, H. D. Hristov, and R. Feick, "Inverted-F antennas wideband match performance," *Electron. Lett.*, vol. 38, no. 16, pp. 845–847, Aug. 2002.

[18] D. M. Pozar, *Microwave Engineering*, 3rd ed. New York, NY, USA: Wiley, 2004.

[19] S. S. Bedair, "Characteristics of some asymmetrical coupled transmission lines," *IEEE Trans. Microwave Theory Tech.*, vol. MTT-32, pp. 108–110, 1984.

[20] F. E. Terman, *Radio Engineers' Handbook*. New York, NY, USA: McGraw-Hill, 1943.

[21] J. Oh and K. Sarabandi, "A topology-based miniaturization of circularly polarized patch antennas," *IEEE Trans. Antennas Propag.*, vol. 61, no. 3, pp. 1422–1426, Mar. 2013.

[22] J. Oh, J. Choi, F. T. Dagefu, and K. Sarabandi, "Extremely small two-element monopole antenna for HF band applications," *IEEE Trans. Antennas Propag.*, vol. 61, no. 6, pp. 2991–2999, Jun. 2013.